THE JOURNAL OF PHYSICAL CHEMISTRY C

Article

Cite This: J. Phys. Chem. C 2020, 124, 997−1007

pubs.acs.org/JPCC

Experimental and ab Initio Studies of Deep-Bulk Traps in Doped Rare-Earth Oxide Thick Films

Leandro S. R. Rocha,*[,†] Federico Schipani,[§] Celso M. Aldao,[§] Luis Cabral,[‡] Alexandre Z. Simoes,[∥] Carlos Macchi,[⊥] Gilmar E. Marques,[‡,§] Miguel A. Ponce,[†,§] and Elson Longo[†]

[†]Department of Chemistry and [‡]Department of Physics, Federal University of São Carlos, São Carlos 13565-905, Brazil

[§]Institute of Materials Science and Technology (INTEMA), University of Mar Del Plata and National Research Council (CONICET), Mar Del Plata 7600, Argentina

[∥]School of Engineering, São Paulo State University (UNESP), Guaratinguetá 01049-010, Brazil

[⊥]Instituto de Física de Materiales Tandil (UNCPBA) and CIFICEN (UNCPBA-CICPBA-CONICET), Tandil 399 7000, Argentina

ABSTRACT: Lanthanum-doped CeO_2 is a promising semiconductor for gas sensing. A combined study applying impedance spectroscopy and first-principles calculations was performed for pure and lanthanum-doped samples. The results showed a strong influence of the localized Ce 4f states on the electrical conduction processes and an electrical resistance increase as a function of the exposure to vacuum and air atmospheres. After its modification with a rare-earth element along with exposure to reducing and oxidizing atmospheres, the observed behavior suggested the presence of multitraps, which depended on the described equilibrium between the oxygen vacancies ($V_o^x \leftrightarrow V_{O^\cdot} \leftrightarrow V_{O^{\cdot}}$) in a disordered deep-bulk trap location. According to the DFT results, the multitraps were formed with the creation of an oxygen vacancy far from the doping atom. They were considered to be responsible for the phenomena modifying the Debye-like response. The transfer of electrons from Ce(III) to the adsorbed oxygen species, decreasing the number of electrons in the 4f state, reduced the electrical conductivity by the hopping frequency dependence of the total resistance and capacitances. This was probably due to the interactions between defective oxygen and metallic species.

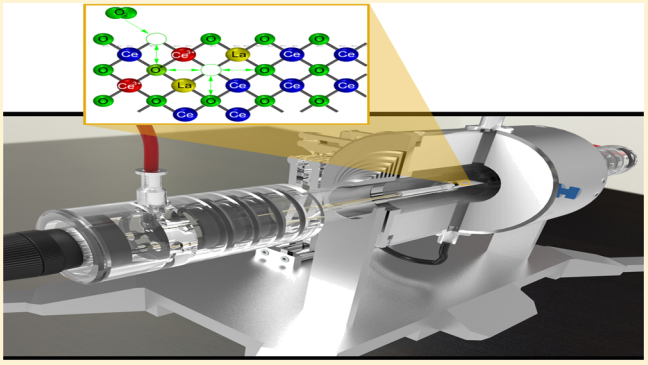

1. INTRODUCTION

Nanostructured rare-earth doped semiconductor oxides have attracted tremendous attention due to potential for multifunctional applications, ranging from solid oxide fuel cells (SOFCs)[1] to gas sensors[2] and photocatalysts.[3] In fact, doped ceria (CeO_2) is one of the most attractive rare-earth oxides particularly owing to its high ionic conductivity at relatively low temperatures (<800 °C)[4] combined with a high chemical stability,[5] advancing its use in various fields.

Monocrystalline CeO_2 crystallizes as a fluorite structure ($Fm\bar{3}m$) and presents a band gap (E_g) of 6 eV (O 2p → Ce 5d), as measured by optical reflectance[6] with oxygen vacancies ($V_{O^\cdot}$) as the predominant ionic defects.[7] Doping CeO_2 with low-valence compounds introduces oxygen vacancies in the structure along with a slight distortion in the local structure,[8] playing an important role in determining its overall physicochemical properties. Indeed, a study of the ionic conductivity of CeO_2 doped with different rare-earth elements suggested that rare-earth doping plays multiple roles in increasing the oxygen vacancies.[9] Because of this modification, the Ce 4f states can be occupied or unoccupied with a redox (reduction/oxidation) process of $Ce^{+4} \rightarrow Ce^{+3}$. The ionic nature of the oxygen vacancies plays a key part in their capability to reduce or increase their oxidation states because the step that controls the redox rate, the oxygen diffusion, depends on their type, size, and concentration.[10] This indicates that different processing conditions may favor the formation of more desired oxygen vacancies, thereby resulting in distinct improved properties, intrinsically related to their applicability. Hence, understanding these vacancies and defects is required.

In dealing with rare-earth oxides with 4f shells, we must consider the presence of localized states at the semiconductor band gap. In addition, the presence of ionized oxygen vacancies as the predominant defects in these non-stoichiometric systems must be considered. These vacancies, which donate electrons to the localized states at the semiconductor band gap, are also responsible for the generation of small polarons. A small polaron is a defect created when an electronic carrier becomes trapped at a given site because of the displacement of adjacent species. The entire defect (carrier

Received: July 29, 2019
Revised: December 2, 2019
Published: December 3, 2019

DOI: 10.1021/acs.jpcc.9b07217
J. Phys. Chem. C 2020, 124, 997−1007

plus distortion) then migrates via an activated hopping mechanism. This phenomenon can occur in materials whose conduction electrons belong to incomplete inner (d or f) shells, which display a slight electron wave-function overlap and tend to form extremely narrow bands. The presence of electrons in these localized states leads to an electrical conduction based on the hopping mechanism.[11,12] Non-stoichiometric oxides such as PrO_{3-x}, TbO_{2-x}, and CeO_{2-x}, which have fluorite-type structures, are interesting semiconductors with their x composition varying over a wide range (from 0 to 0.5) with reduction, that is, with the control of the oxygen partial pressure (p_{O2}) during the synthesis.[13] In addition, CeO_2 has the following two advantages over other oxides:

(a) It offers the best opportunity to achieve the theoretically simple case where the x concentration of electrons is small.
(b) Its electronic structure is simple because the Ce^{4+} species in CeO_2 has an empty 4f shell that starts to become occupied only under redox processes.

Therefore, the removal of oxygen species facilitates in donating electrons to the bulk of the semiconductor as well as generates ionized oxygen vacancies in the structure, such as $V_{O}^{\cdot}$,$V_{O}^{\cdot}$, and $V_{O}^{\times}$, depicted as multitraps, as represented in Figure 1, which shows the possible oxygen vacancy diffusion

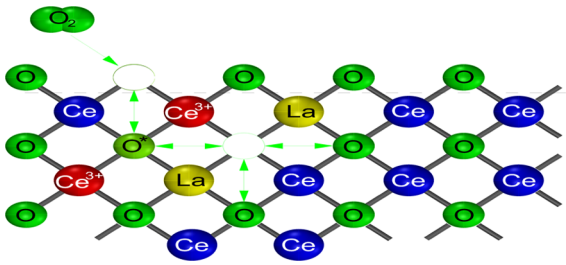

Figure 1. Schematic of the multitraps, represented as oxygen vacancy sites neighboring Ce(III) species.

paths, their interactions between couples of vacancies and with the surrounding atmosphere, and structural relaxations around vacancies. This process of oxygen vacancy generation also creates small polarons, responsible for the hopping conduction mechanism.

Studies by Blumenthal et al.[14,15] indicated that hopping-type conductivity indeed occurred in reduced (CeO_{2-x}) ceria-based systems. In the first investigation,[14] they attempted to hold x constant by purging the system with a purified He gas but found that the readings changed with time, and therefore it was necessary to heat or cool the sample relatively rapidly to avoid changes in the composition. They reported a hopping activation energy (E_a) of 0.22 eV at a low x, which increased with increasing x. In the second study,[15] the conductivity was measured in equilibrium as a function of p_{O2} and compared with separately determined thermogravimetric data for x versus p_{O2}. They claimed that this second method yielded better results than those of the previous nonequilibrium method and reported a slightly smaller value of E_a = 0.16 eV (compared to the first case) for mildly reduced CeO_2.

The valence band of pure CeO_2 is primarily composed of O 2p states, whereas the conduction band is predominantly formed by Ce 5d states with a narrow Ce 4f band in between. The current understanding is that the full Ce 4f states are localized atomic f-like species located at the neighboring vacancies of the cerium atoms (i.e., the three-dimensional electronic density suggests a higher probability of the electron to be found on its first-neighboring oxygen vacancy). Although their exact separation is still not clear, it is suggested that the 4f occupied states may be anywhere in the range of 1.5−2.5 eV above the valence band energy (E_v).[16] This occupancy in the final state may change owing to the charge transfer from valence or conduction bands because of doping, which is a general phenomenon in Ce-based compounds, implying mixed valences of both $4f^0$ and $4f^1$ configurations.[17] Additionally, the modification with rare-earth elements promotes oxygen donation by lowering the necessary energy to form surface anionic vacancies when exposed to a gaseous atmosphere. Subsequently, the two excess electrons are located on the structural species, reducing them to Ce(III) and La(II) once stable mononuclear La(II) compounds can be found.[18] The rare-earth doping also favors the activation of O_2 molecules on the surface of oxygen vacancies, leading to the formation of a superoxide (O_2^-) radical as well as re-oxidation of Ce(III) to Ce(IV).[19]

We have previously reported the optimization regarding the synthesis of pure CeO_2 in terms of distinct mineralizer agents (2 M KOH, NaOH, and NH_4OH)[20] followed by the evaluation of the influence of distinct synthesis times (1, 2, 4, and 8 min) on its microstructural and photoluminescent (PL) properties.[21] Then, the modification with rare-earth elements was also studied with respect to the addition of lanthanum [La(III)] species at 4, 8, and 12 wt % in terms of XRD and Rietveld refinement, Raman, UV−vis, and PL spectroscopies along with SEM analysis.[22] The main goal of lanthanum addition was to induce the creation of defective species causing structural expansion,[23] resulting in the improvement of the gas-sensing properties. The electrical behavior of the pure ceria-based films obtained from the powders synthesized at distinct soaking times was also investigated in the presence of 200 mmHg (0.263 atm) of synthetic air and CO atmospheres in a temperature ranging from 100 to 350 °C. Afterward, the temperature of 350 °C was kept, changing the CO and air atmosphere pressures for 10 (0.013 atm), 50 (0.065 atm), and 200 mmHg (0.263 atm).[24] The gas-sensing measurements of the CeO_2-based thick films presented a dual (electric and optical) gas-sensing behavior when doped with lanthanum on exposure to a carbon monoxide atmosphere at temperatures above 350 °C. This was attributed to the itinerant 4f electrons created after the oxygen vacancy generation. Therefore, the precise role of oxygen vacancies is crucial to develop improved understanding of this important oxide material. However, creation of these favorable defects and understanding their roles in the atomic level activity of nanosized CeO_2 are still lacking. Thus, there is a need to study the vacancy structure of these oxides using a probe that can provide information at the atomic level.

The most important properties found on doping CeO_2 with La were the rapid changes in the electrical and optical responses in comparison with the pure CeO_2, presenting only electrical changes. Once the gas-sensing measurements of the 8 wt % La-doped CeO_2 sample depicted a peculiar dual-sensing behavior,[20] not seen in the pure, 4 wt %, and 12 wt % systems, we have focused our attention on this particular system to specifically study the dependence of rare-earth modification with an ac bias (V) application under vacuum and air (~20% O_2) exposure, differing from the classical Schottky-type

DOI: 10.1021/acs.jpcc.9b07217
J. Phys. Chem. C 2020, 124, 997−1007

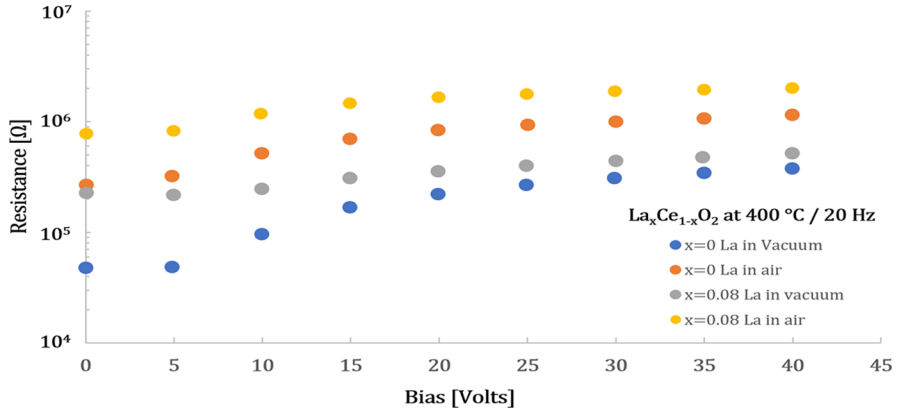

Figure 2. Resistance vs bias (V) for pure and doped samples in vacuum and air atmospheres. Consider the air atmosphere with a 50 mmHg of oxygen partial pressure (p_{O2}).

semiconductors, to determine the most likely conduction mechanism for nanostructured CeO_2-based systems.

Once the core electrons retain their atomic character, even when the atoms form a solid, the experimental results can be directly compared to the theoretical predictions obtained by density functional theory (DFT). Therefore, a mixed theoretical−experimental approach was used to fully comprehend the dependence of rare-earth modification with its dual behavior in an ac bias (V) application under vacuum and air (~20% O_2) exposure to determine the most likely conduction mechanism for nanostructured CeO_2-based systems in terms of capacitance variation in accordance with the hopping conduction mechanism differing from that of classical Schottky-type semiconductors combined with ab initio studies.

2. EXPERIMENTAL SECTION

2.1. Nanomaterial Preparation and Characterization. The complete description regarding the nanopowder preparation by the microwave-assisted hydrothermal (MAH) method as well as the film fabrication via a handmade simple deposition is thoroughly and precisely reported in several works.[25−27]

CIS of the films was performed using an HP4284A impedance analyzer in a closed "device for the optoelectronic characterization of materials" under a patent in Brazil (no. BR102016028383) and Argentina (no. AR103692). The measurements were made at 200 and 400 °C, owing to the color change phenomenon occurring in the 8 wt % La-doped CeO_2 sample.[25] Atmosphere changes were conducted with three different oxygen partial pressures (p_{O2}) from vacuum (10^{-3} mmHg or 1.33×10^{-6} bar) to 10 mmHg (0.013 atm) and 50 mmHg (0.065 atm) of synthetic air (20% O_2). For the atmosphere exposure analysis, an applied magnitude of excitation current of 1 mA was used with the two-point probe technique in an ac-type measurement on a frequency interval of 10 Hz−1 MHz.

It is worth mentioning that owing to the applied current range, the samples present an Ohmic behavior, and the electrodes' capacitance contribution can be ignored. To ensure that the electric response was exclusively generated by the exposure to the different atmospheres, the films were thermally treated thrice (3×) in a closed atmosphere of dry synthetic air up to 380 °C with a 1 K/min rate and kept for 2 h. Therefore, no traces of humidity or even glycerol (boiling point at 760 mmHg: 563 K[28]) influenced the measurements.

2.2. Theoretical Approach and Computational Details. Our ab initio investigations are based on DFT[29,30] calculations employing the semi-local Perdew−Burke−Ernzerhof[31] exchange and correlation energy functional within the spin-polarized generalized gradient approximation (GGA) formulation. The Kohn−Sham equations were solved by using the all-electron projector augmented plane wave (PAW) method,[32,33] which employed the following projectors Ce($4f^1$, $5d^1$, $6s^2$), O($2s^2$, $2p^4$), and La($5d^1$, $6s^2$) where the valence states are shown in parentheses. The calculations were performed with the Vienna ab initio simulation package (VASP),[34,35] version 5.4.4. The equilibrium volume of the CeO_2 unit cell was reached by the minimization of the stress tensor by employing a plane wave basis with a kinetic energy cutoff of 829 eV. In addition, for the atomic force optimizations, a plane wave basis with a cutoff of 466 eV was used, which was 12.5% higher than the value recommended by the VASP package. A *k*-mesh of 2 × 2 × 2 was used once to integrate the Brillouin zone for the stress tensor and atomic force optimizations and twice for the electronic properties. A Gaussian smearing of 0.01 eV was employed in all the calculations, and the atoms were allowed to relax until all the forces were smaller than 0.01 eV/A on each atom. To obtain a better description of the large CeO_2 energy gap and band structure, we adopted the Hubbard correction (GGA + *U*) method[36] where *U* parameters are 4.50, 5.0, and 5.50 eV on f-La, f-Ce, and p-O states, respectively, in accordance with the literature.[33,34]

3. RESULTS AND DISCUSSION

3.1. Complex Impedance Spectroscopy (CIS). The resistance versus bias (V) dependence for the pure and La-doped films can be seen in Figure 2, depicting the effect of the lanthanum addition on the electrical resistance of the films with a lower valence state of La^{3+} (r = 0.110 nm) than Ce^{4+} (r = 0.097 nm) at distinct applied voltages. A mild dependence of resistance (Ω) versus bias (V) can be observed at Figure 2, and it is related to the voltage coefficient of resistance (VCR), expressed as the ratio of the resistance change in ohms to the corresponding increase in the applied voltage in volts when the temperature is constant. Most resistors have a negative VCR,[39] which implies that at high voltages, the resistance decreases during the pulse. However, a reduction in the electrical conductivity is observed for both vacuum and air atmospheres in the entire range along with a structural expansion after

DOI: 10.1021/acs.jpcc.9b07217
J. Phys. Chem. C 2020, 124, 997−1007

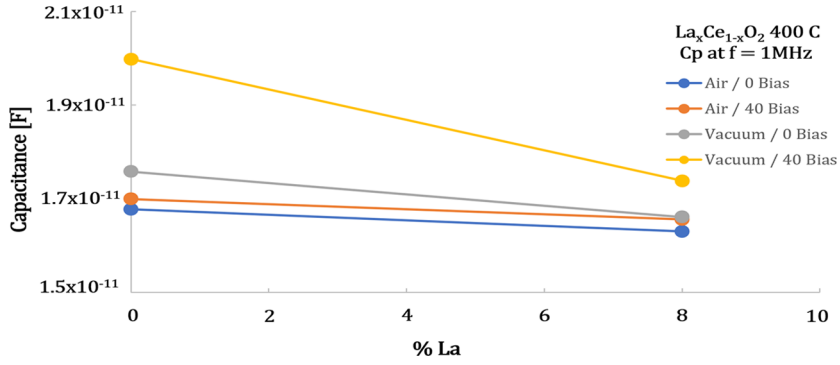

Figure 3. Capacitance of *x*% La for distinct applied voltages and atmospheres.

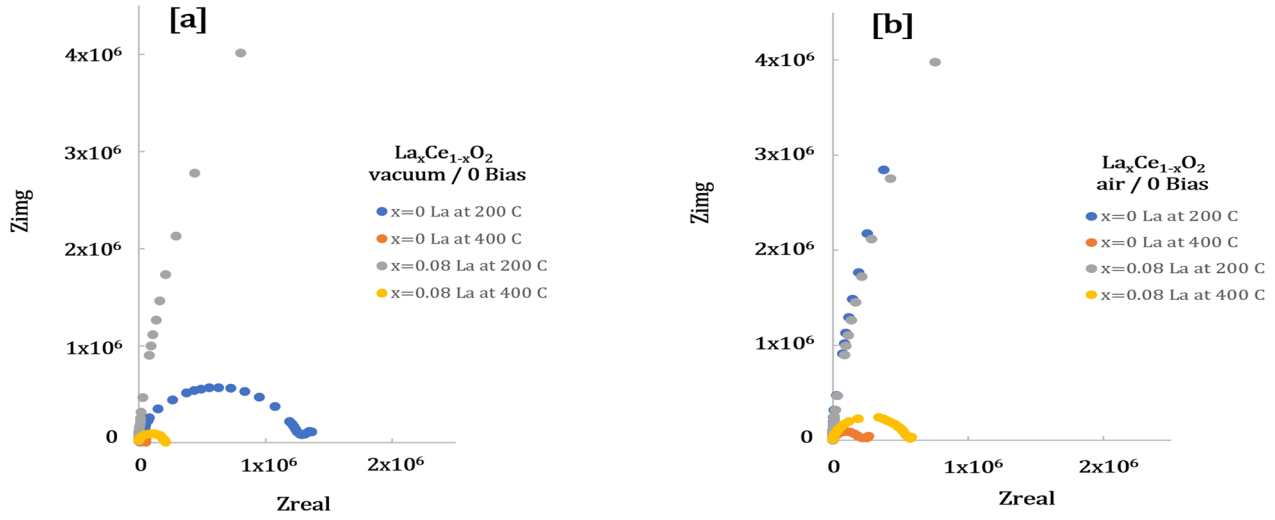

Figure 4. Impedance plots for the pure and doped systems in (a) vacuum and (b) air at 0 V for 200 and 400 °C.

lanthanum addition.[23] This indicates that our samples present a positive resistance coefficient with a remarkable dependence for the pure CeO_2 film, increasing its resistance for the high-voltage regime. The modification with La decreased the positive VCR behavior, which depends not only on the length of the resistor but also on the conductive interfaces between the particles, which can lead to emission of charge carriers across particle gaps via hopping conduction.

Additionally, the modification with lanthanum increases the electrical resistance in the entire voltage range, although the VCR decreases. This behavior can be interpreted as a consequence of the decrease in the number of Ce(III) species on the film surface. Details regarding the intermediate and high-voltage regimes are found to depend strongly on the doping density and energy distribution of the defect states because the current−voltage nonlinearities found in real materials are most probably associated with the defect-state densities, which decrease at an above zero bias.[40] In fact, doping CeO_2 with lanthanum generates more ionized oxygen vacancies. Once CeO_2-based films present hopping electrons localized at the 4f states, corresponding to Ce(III) species, La^{3+} doping changes the oxidation of the Ce(III) species to Ce(IV), shifting down the Fermi level. Thus, few electrons in the 4f states are available for electrical conduction, thereby increasing their total electrical resistance.

In previous work, structural evidence has been used to deduce that the distribution of La^{3+} in the CeO_2 structure is random[41] and, in particular, that the formation of oxygen vacancies[42,43] is accompanied by a reduction of the Ce^{4+} to Ce^{3+} states. Following the findings of Heinmaa et al.[37] regarding oxygen anion migration, O'Neill and Morris[38] further supported the concept that oxygen anions are mobile and distributed randomly throughout the CeO_2 structure. Contrastingly, phenomena associated with oxidation from the Ce^{3+} to Ce^{4+} states have been reported[44] because of the oxygen exchange between the ambient gas-phase oxygen and structural oxygen in the oxide. Indeed, this oxidation from Ce^{3+} to Ce^{4+}, along with an increase of 8% in the defective oxygen species, according to XPS analyses, is seen in our previous report (under review, APSUSC-D-19-13517) due to the modification with lanthanum.

To study the gaseous adsorption phenomena and the induced changes in the carrier concentration, we analyzed the film grain boundary capacitances obtained at a frequency of 1 MHz from the total parallel capacitance.[45] This study is shown in Figure 3. The non-overlapping barriers in semiconductors are related to changes in the grain boundary capacitance during bias measurements when the conduction mechanism considers parabolic-type potential barriers on the grain surface (band bending). For the CeO_2 samples, we must consider that the hopping of electrons between 4f states is responsible for the electrical conduction along with the intermediate energy levels[46] because of the large 6 eV band gap.

After exposure to the air atmosphere, the capacitance (C_p) shows a slight decrease for the increasing La-doped system. This can be interpreted as an exchange interaction between

DOI: 10.1021/acs.jpcc.9b07217
J. Phys. Chem. C 2020, 124, 997−1007

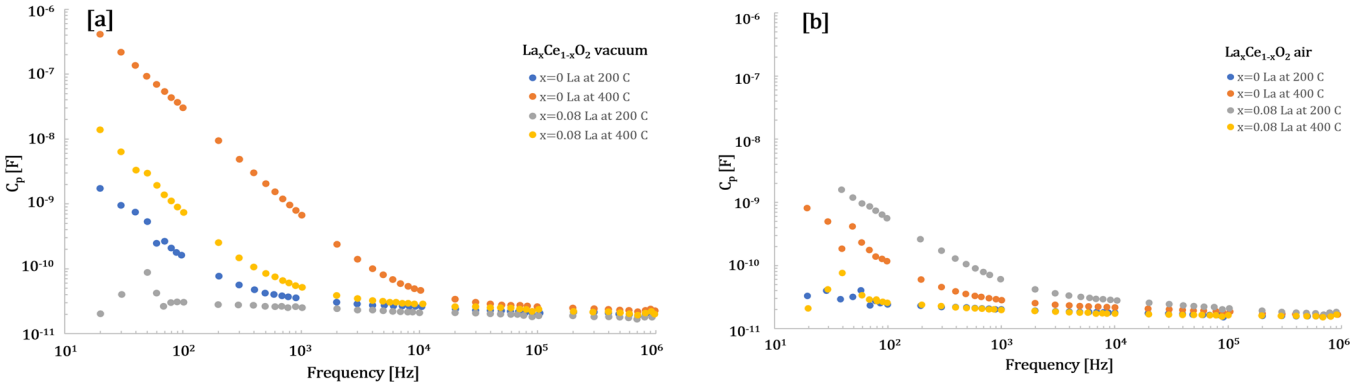

Figure 5. Capacitance (C_p) vs frequency (Hz) in (a) vacuum and (b) air atmospheres.

oxygen species in the air atmosphere with the CeO_2 structure, annihilating the oxygen vacancies. This process reduces the number of charge carriers and thereby the capability to store charges. After the modification with lanthanum, the film capacitances in both the atmospheres and at the applied voltages were reduced, indicating a decrease in the density of the defective Ce(III) species that possess itinerant 4f electrons responsible for the electrical hopping conduction mechanism. This is a typical behavior presented in semiconductor oxides where the number of defective species is decreased as the bias increases, in good agreement with previous work explaining the semiconductor oxide capacitance dependence on the applied voltages.[47] It is worth mentioning that the solid lines used to connect the 0 and 8 wt % points serve only as guides to give higher contrast in the figure once the observed trends with distinct amounts of La do not present a linear behavior as shown in the following measurements.

In Figure 4a,b, pure and La-doped CeO_2 impedance plots are presented for 200 and 400 °C in vacuum and oxygen-rich atmospheres. This is done to analyze the influence of the adsorbed oxygen species on the film surface and their diffusion into the grains along with the consequent annihilation of the oxygen vacancies and reduction in the donor concentration. The opposite phenomena occur when oxygen diffuses out of the grains, generating vacancies, as in the case of the interaction with $CO_{(g)}$. The relevant reactions for the oxygen species from the gas phase to the bulk of the grain are thoroughly reported elsewhere.[46,48] However, if the surface is treated with a reducing atmosphere, the oxygen species migrates to the surface generating oxygen vacancies in an exchange process.[44]

It can be seen that the conduction is thermally favored in both samples once the semicircle diameter is reduced at 400 °C. The lanthanum-doped sample presents a larger impedance than that of the pure system in both temperatures, indicating a decrease in the number of 4f electrons available for conduction. The introduction of a trivalent lanthanum (La^{3+}) in the structure promotes the creation of a relatively higher number of oxygen vacancies along with a narrowing of the energy of the Fermi level and valence band (E_F–E_v). These two phenomena can induce opposite effects on the final electrical resistance of the samples with the vacancy generation increasing the number of electrons in the 4f states along with the conductivity. Contrastingly, if the Fermi level (E_F) moves down, then E_{4f}–E_F increases and sample conductivity decreases. These phenomena were also observed in a previous work where a europium-doped CeO_2 sample presented a slightly small band gap value of 3.26 eV, becoming less conductive compared to the pure sample.[26]

By comparing Figure 4a,b, we can deduce the interaction of oxygen with the grain surfaces, which finally reduces the number of $4f^1$ electrons. A large impedance increase is observed for pure and doped samples exposed to air atmospheres at 200 and 400 °C when compared to the vacuum atmosphere. The oxygen interaction with the surface causes a transfer of electrons from the bulk ($4f^1$ states), which also modifies the energy difference between the Fermi level and 4f state at the band gap (E_{4f}–E_F). The density of the carriers decreases and, consequently, the sample impedance increases with doping in both temperature regimes. Hence, the introduction of lanthanum in the structure imposes a narrowing effect on the energy gap (E_F–E_v), causing an increase in the sample resistivity because of the relatively larger number of bulk Ce(IV) species with no 4f electrons available for conduction.

The capacitance dependence on the frequency for the pure and doped samples in vacuum and air atmospheres at 200 and 400 °C can be seen in Figure 5a,b.

The observed behavior suggests the possible presence of multitraps, which depends on the described equilibrium between the oxygen vacancies ($V_{O^x} \leftrightarrow V_{O^{\cdot}} \leftrightarrow V_{O}$) in the CeO_2 samples with a $1/f^2$ (Hz) dependence of C_p. The latter shows an inflection point corresponding to a critical frequency, named "corner frequency",[46] with a disordered deep bulk trap location. The multitraps are considered responsible for the phenomenon that modifies the Debye-like response. When dealing with a distribution of activation energies and not a single activation energy, one shifts from a simple ideal resistor and capacitor in a parallel case to a distribution of impedance elements (constant-phase element, CPE). Deep traps are activated with temperature as shown by the dependence of the square of the frequency for the samples exposed to vacuum and air atmospheres. Contrarily, the modification with lanthanum decreases the effect of the deep and shallow traps with frequency. Additionally, at the high frequencies, virtually no dependence of the capacitance on frequency at 200 and 400 °C can be seen for both samples. Indeed, for the higher values, the sample capacitances have a mild dependence on the frequency. This behavior is consistent with the absence of band bending or with the band bending not affecting the sample capacitance. Deep bulk traps are affected by the doping, temperature, and atmosphere exposure, as shown in Figure 5a,b. When the samples are exposed to an air atmosphere, a decrease in the deep bulk-trap distribution is observed at low

DOI: 10.1021/acs.jpcc.9b07217
J. Phys. Chem. C 2020, 124, 997–1007

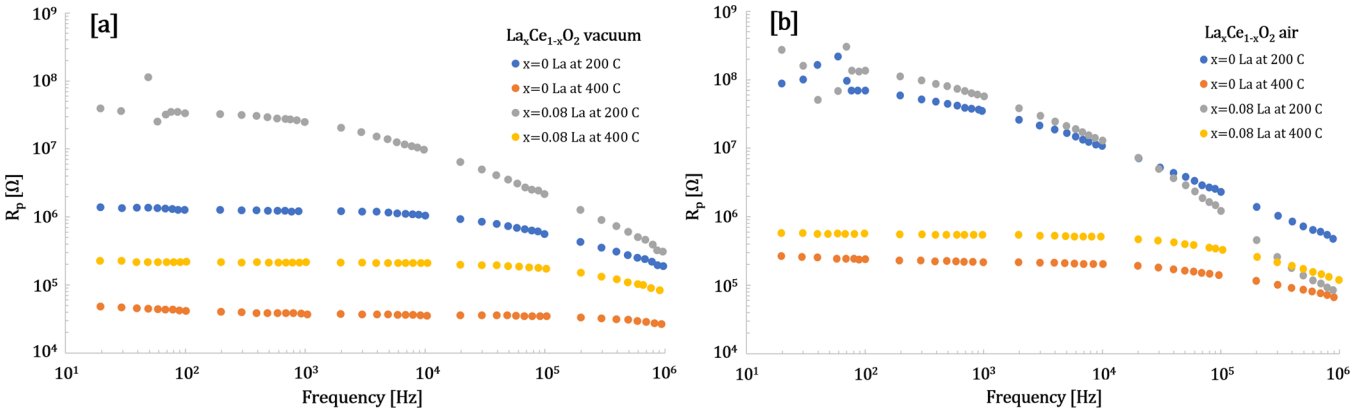

Figure 6. Resistance (R_p) vs frequency (Hz) in (a) vacuum and (b) an air atmosphere.

frequencies. This can be probably ascribed to trap deactivation because the samples are exposed to air owing to the slight shift of the Fermi level to relatively lower positions due to exchange interactions with the oxygen species.[44]

The drop in the resistance with temperature, as seen in Figure 6, can be associated with the modification of the carrier transport because all transport mechanisms are facilitated with temperature. Under the experimental conditions in which the sample is exposed to vacuum and temperature is altered, a variation in the barrier height or width would not be possible. Therefore, the electronic hopping transport mechanism must be responsible for the observed changes in the resistance. These results are consistent with previous reports for polycrystalline semiconductors.[48] The observed Fermi level energy decrease with lanthanum modification increases the film resistance, as previously observed.

A mild dependence of the resistance with frequency is shown mostly at 200 °C by both the pure and doped samples at frequencies higher than 10 kHz. This indicates a behavior that cannot be appropriately described by a simple RC equivalent circuit and therefore probably need an electrical circuit representation including the presence of multitraps[41] corroborating the presence of defective oxygen species, such as vacancies. Therefore, we show that the frequency dependence of the total resistance and capacitance can be assigned to the presence of deep bulk traps, which are probably ascribed to the interactions of the defective oxygen and metallic species throughout the system.

As the antimatter equivalent of an electron, a positron is an extremely nondestructive sensitive probe of both the structural and electronic properties of solids. Among the different experimental variants of the positron annihilation spectroscopy (PAS), positron annihilation lifetime spectroscopy (PALS) has demonstrated to be the most adequate technique to study vacancy-like defects, providing quantitative sensitivity and selectivity to this type of defect.[45] Recently, several researchers used PALS to study the defect structure in different CeO_2-based nanostructured systems.[46−49] In particular, Liu et al.[49] studied the influence of the defect structure on the catalytic activity of two CeO_2 nanorod samples synthesized using different methods. Moreover, Wang et al.[50] reported results on the role of oxygen vacancies in the catalytic performance for *o*-xylene oxidation of CeO_2 nanocubes calcinated at different temperatures. In both cases, the authors reported the formation of small neutral Ce^{3+}−V_O associations, defined as $[Ce'Ce−V_O·-Ce'_{Ce}]^x$, and large oxygen vacancy clusters. By contrast, Sachdeva et al.[51] studied the defect structure in $Ce_{1-x}Nd_xO_{2-x/2}$ nanostructured samples with x ranging from 0.076 to 0.675. For nominal Nd concentrations lower than 0.4, the authors proposed the formation of neutral Nd−oxygen vacancy clusters defined as $[Nd'_{Ce}−V_{O·}—Nd'_{Ce}]^x$. Similarly, Thorat et al.[52] reported a systematic study of the defects generated in samples of nanostructured CeO_2 samples doped with different concentrations of Eu ranging from 0 to 50 at. %. In this work, the authors reported that, for Eu concentrations lower than 1%, the dominant defects were Ce^{3+}−V_O-type associates. At relatively higher Eu concentrations, these associates agglomerated to form larger V_O clusters including Ce^{3+} and Eu^{3+} species. Furthermore, the preliminary PALS results measuring the nanostructured pure and lanthanum-doped CeO_2 samples indicated that the defect structures of these samples were consistent with the existence of the vacancy-like associates described hereafter.

To understand the interaction between the vacancy defects and metal species, we must first consider the resonant equilibrium between the ordered and disordered $[CeO_8]$ clusters, represented as

$$[CeO_8]_o^x \leftrightarrow [CeO_8]_d^x \quad (1)$$

Then, we can consider the intrinsic generation of oxygen vacancies such as

$$[MO_8]_o^x + [MO_8]_d^x \rightarrow [MO_8]_o' + [MO_7·V_{O·}] + 1/2O_2 \quad (2)$$

$$[MO_8]_o^x + [MO_7·V_O·] \rightarrow [MO_8]_o' + [MO_7·V_O··] \quad (3)$$

$$[MO_8]_o^x + [MO_7·V_O^x] \rightarrow [MO_8]_o' + [MO_7·V_O·] \quad (4)$$

$$[MO_7·V_O^x] + [MO_7·V_O·] \rightarrow [MO_7·V_O^x]_o' + [MO_7·V_O··] \quad (5)$$

where M represents a rare-earth element. The ab initio studies indicate that, under oxygen-poor conditions, the defects with the lowest formation energy are oxygen vacancies, whereas oxygen interstitials, which form peroxide ions, will be more favorable under oxygen-rich conditions, with oxygen vacancies typically being the dominant defect.[38] Additionally, the interaction of an oxygen vacancy with one or two substitutional elements will depend on the radius size of the dopant with a first-neighbor interaction occurring for small elements and a second-neighbor interaction occurring with large dopants. Once the experimental measurements were performed with an oxygen partial pressure (p_{O2}) of up to 0.065 atm and an air

DOI: 10.1021/acs.jpcc.9b07217
J. Phys. Chem. C 2020, 124, 997−1007

atmosphere can be considered when p_{O2} = 0.2 atm, we can admit our experimental parameters as under oxygen-poor conditions with oxygen vacancies being the most likely defects.

In an air atmosphere, the interaction of oxygen species with these clusters can be probably considered as:

$$[MO_7{\cdot}V_O^{z}] + O_2 \rightarrow [MO_7{\cdot}V_O^{z}]\cdots O_{2(ads)} \text{ where } V_O^{z} = V_O^{x}, V_O{\cdot}, \text{ or } V_O{\cdot}{\cdot} \quad (6)$$

$$[MO_7{\cdot}V_o^{x}]\cdots O_2 \rightarrow [MO_7{\cdot}V_O{\cdot}]\cdots O'_{2(ads)} \quad (7)$$

$$[MO_7{\cdot}V_O{\cdot}{\cdot}] + O_2 \rightarrow [MO_7{\cdot}V_O{\cdot}{\cdot}]\cdots O_{2(ads)} \quad (8)$$

We must also consider that different oxygen species can be formed depending on the working temperature.[50] For CeO_2 clusters, we can rewrite eqs 6 and 7 as

$$[CeO_7{\cdot}V_O^{x}]\cdots O_{2(ads)} \rightarrow [CeO_7{\cdot}V_O{\cdot}]\cdots O_2'(ads) \quad (9)$$

$$[CeO_7{\cdot}V_O{\cdot}]\cdots O_2 \rightarrow [CeO_7{\cdot}V_O{\cdot}]\cdots O'_{2(ads)} \text{ for } T > 573 \text{ K} \quad (10)$$

The ionized oxygen species adsorbed on the CeO_2 surface can also be represented by eqs 9 and 10. We can also consider the transfer of an electron from Ce(III) to the oxygen species, decreasing the number of electrons in the 4f states and reducing the electrical conductivity by hopping. This occurs according to the following steps, which differ depending on the ceria cluster interacting directly with the oxygen molecules in the atmosphere. In this case, the presence of Ce'_{Ce}-type species, which represent the presence of Ce(III) can be considered as polarons, which likely contribute to the electrical conduction mechanism.[51]

$$[CeO_7{\cdot}V_O^{x}]\cdots O_{2(ads)} + [CeO_8]_o' \rightarrow [CeO_7{\cdot}V_O^{x}]\cdots O_2' + [CeO_8]_o^{x} \quad (11)$$

$$[CeO_7{\cdot}V_O{\cdot}]\cdots O_{2(ads)} + [CeO_8]_o' \rightarrow [CeO_7{\cdot}V_O{\cdot}]\ldots O_2' + [CeO_8]_o^{x} \quad (12)$$

$$[CeO_7{\cdot}V_O{\cdot}{\cdot}]\cdots O_{2(ads)} + [CeO_8]_o' \rightarrow [CeO_7{\cdot}V_O{\cdot}{\cdot}]\cdots O_2' + [CeO_8]_o^{x} \quad (13)$$

$$[CeO_7{\cdot}V_O^{x}] + [CeO_7{\cdot}V_O{\cdot}]\cdots O_2 \rightarrow [CeO_7{\cdot}V_O{\cdot}]\cdots O_2' + [CeO_7{\cdot}V_O{\cdot}] \quad (14)$$

For the lanthanum-doped sample, we must also consider the presence of lanthanum complex clusters, represented as follows

$$[LaO_8]_o^{x} + [LaO_7{\cdot}V_O^{x}] \rightarrow [LaO_8]_o' + [LaO_7{\cdot}V_O{\cdot}] \quad (15)$$

$$[LaO_8]_o^{x}\cdots[LaO_7{\cdot}V_O^{x}] \rightarrow [LaO_8]_o'\cdots[LaO_7{\cdot}V_O{\cdot}] \quad (16)$$

$$[CeO_8]_o^{x}\cdots[LaO_7{\cdot}V_O^{x}] \rightarrow [CeO_8]_o'\cdots[LaO_7{\cdot}V_O{\cdot}] \quad (17)$$

$$[CeO_8]_o' + [LaO_7{\cdot}V_O{\cdot}] \rightarrow [CeO_7{\cdot}V_O{\cdot}] + [LaO_8{\cdot}]_o' \quad (18)$$

We can also consider a doubly ionized oxygen vacancy formation that does not lead to an electrical resistance change, although it can correspond to an excellent positron trapping site. This doubly ionized oxygen vacancy formation can be expressed as

$$[LaO_8]_o^{x}\cdots[CeO_7{\cdot}V_O^{x}]\cdots[LaO_8]_o^{x} \leftrightarrow [LaO_8]_o'\cdots[CeO_7{\cdot}V_O{\cdot}{\cdot}]\cdots[LaO_8]_o' \quad (19)$$

Additionally, the contribution of the oxidation state fluctuation for the lanthanum atoms should be considered, as represented in the equation below. It can also lead to a positron trapping site but does not increase the sample resistance.

$$[LaO_8x]_o'\cdots[CeO_7{\cdot}V_O{\cdot}]\cdots[LaO_8]_o^{x} \rightarrow [LaO_8]_o'\cdots[CeO_7{\cdot}V_O{\cdot}{\cdot}]\cdots[LaO_8]_o' \quad (20)$$

The following equation represents the increase in paramagnetic species, when the samples are doped, along with an increase in the number of defective clusters and decrease in Ce^{3+} species, as previously referenced. This equation is confirmed in the experimental measurements and theoretical investigation.

$$[CeO_8]_o' + 2[LaO_8]^{x} + [CeO_7{\cdot}V_o^{x}] \leftrightarrow [CeO_8]_o^{x} + [LaO_8]_o'\cdots[CeO_7{\cdot}V_O{\cdot}]\cdots[LaO_8]_o' \quad (21)$$

3.2. Ab Initio Studies. The use of ab initio calculations allows getting a precise microscopic scenario of electronic levels distribution of pure and rare-earth-doped ceria.[56] Žguns and co-workers[57] found that, for Gd-doped CeO_2, there exists a transition temperature (T_c) below which phase separation into C-type Gd_2O_3 and pure CeO_2 occurs. In the thermodynamic equilibrium, they observed two transitions: the onset of oxygen−vacancy (O−Va) ordering at ca. 1200−3300 K for concentrations of x_{Gd} = 0.3−1, and a phase separation into CeO_2 and C-type Gd_2O_3 occurring below ca. 1000 K for all concentrations. They also modeled "quenched" systems with cations immobile below 1500 K and observed that the presence of random-like cation configurations did not prevent C-type vacancy ordering. The phase separation was observed in the whole studied concentration range (x < 25 wt % Gd) and the transition temperature increased with concentration from ca. 600 (x_{Gd} = 0.03) to 1000 K (x_{Gd} = 0.25). Above T_c, the distribution of Gd is random with oxygen vacancies clustering in the coordination shells along (1, 1/2, 0) and (1, 1, 1) and the nearest neighbor position being preferred for Gd vacancy.[58] Koettgen and co-workers pointed out that the ionic conductivity is influenced by trapping, blocking, and vacancy−vacancy interactions.[59−61] The blocking mechanism mainly limits the dopant fraction at the ionic conductivity and is generally strongly underrated in the literature. Trapping mainly limits the maximum ionic conductivity value with the association energy differences being decisive. The trapping predominantly influences the maximum ionic conductivity as well as the apparent activation enthalpy. The highest conductivity can be found if all absolute values of the association energy differences are small. The rare-earth−vacancy (RE−V) association leads to the formation of associates, that is, vacancies are held by the dopants as their movement is hindered. The long-range RE−V association catches vacancies into the vicinity of dopants. Both the "catch" and "hold" need to be small for a large ionic conductivity. The catch-and-hold principle easily predicts the dopant that leads to the highest ionic conductivity.

According to our investigations, the calculated lattice parameter by using the Hubbard model for the CeO_2 pristine

DOI: 10.1021/acs.jpcc.9b07217
J. Phys. Chem. C 2020, 124, 997−1007

cubic unit cell with the space group $Fm\bar{3}m$ is 5.47 Å, whereas the experimental value is 5.41 Å, a deviation of only 0.06 Å. To avoid the interaction between neighboring images, our calculations were performed by using a CeO_2 supercell extended in two of the three Cartesian directions with one lanthanum atom replacing one cerium in the bulk. There are 63 O (red), 31 Ce (purple), and 1 La (black) atoms, corresponding to a 3.2% La-impurity concentration and the structure having an oxygen vacancy, as depicted in Figure 7.

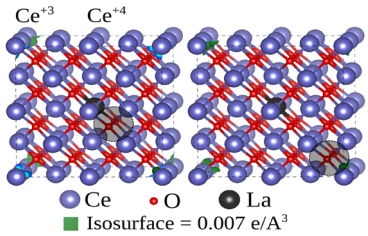

Figure 7. Calculated bulk structures for a lanthanum-doped cerium oxide with one oxygen vacancy.

The oxygen vacancies are placed near (left panel) and far (right panel) from the lanthanum atom in the bulk. In the pristine supercell, each cerium atom is surrounded by eight oxygen atoms. Aiming to investigate the localized magnetic moments, we calculated the spin charge density, $\Delta\rho = \rho\uparrow - \rho\downarrow$, by using an isosurface of +0.007 e/Å^3, as depicted in the same panel. In these calculations, a strong localized magnetic moment appears on one cerium atom of the supercell, which varies the oxidation state of cerium and is responsible for the consequent generation of defective clusters that improve the electrical response and likely creates the optical emission phenomena when exposed to a CO atmosphere. The position of this localized magnetic moment depends on the oxygen vacancy position, as shown in Figure 7. The localized magnetic moment on the cerium atom indicates the presence of Ce^{+3} and oxygen vacancies, which varies the conductivity of the material in agreement with our experimental results. In these calculations, we observe that the presence and position of the oxygen vacancy are crucial to determining the localized magnetic moment on a specific cerium atom. Thus, for a proximal (distant) oxygen vacancy from the lanthanum atom, the localized magnetic moment appears far (near) from the vacancy, as shown in Figure 6. Similarly, the study of defects is a dominating factor for the symmetry of the geometry, which can modify the magnetic ordering of the supercell atoms.

In addition, the electronic properties were investigated by using the calculated density of states per atom, as depicted in Figure 8, for the previously presented structures. In Figure 8, the left (right) panel depicts CeO_2 doped by a lanthanum atom with one oxygen vacancy near (far) from the impurity. It is worth mentioning that the consideration of an oxygen deficiency far from the lanthanum atom, corresponding to the experimental behavior of a more resistive sample, can be represented by eq 18 where the Ce^{3+} specimen is depicted by $[CeO_8]_o'$. In fact, when we think of nanostructured CeO_2-based systems, the tiniest change of the first-neighboring atoms would create distinct dipole moments with differing electronic densities (e.g., Ce(III)−Ce(III), Ce(III)−Ce(IV), Ce(III)−La(III), and Ce(IV)−La(III)), not to mention rare-earth−vacancy (RE−V) interactions. Besides, one can also consider the break of local symmetry, which has direct consequences on the electrical band gap, leading to a distinct density of states as shown in Figure 8.

For both structures, the dominant contributions for the occupied electronic states are given by p-La, p-O, and f-Ce, while the major contributions for unoccupied states are d-La, f-La, p-O, d-Ce, and f-Ce. Note that, in the cerium density of states, the isolated f-Ce spin-up state depicts the localized magnetic moments of Ce^{+3} atoms, as depicted in Figure 7. Thus, the occupied f-Ce electronic states near the Fermi energy is in agreement with the presence of 4f-electrons proposed as the hopping electrical conduction mechanism for the samples.

According to the experimental results given in Section 3.1, after modification with lanthanum, the sample becomes more resistive in both the vacuum and air atmospheres, being a good indicator that the electrons from the Ce $4f^1$ states decay to the La f-states (shown in Figure 8). Additionally, ab initio

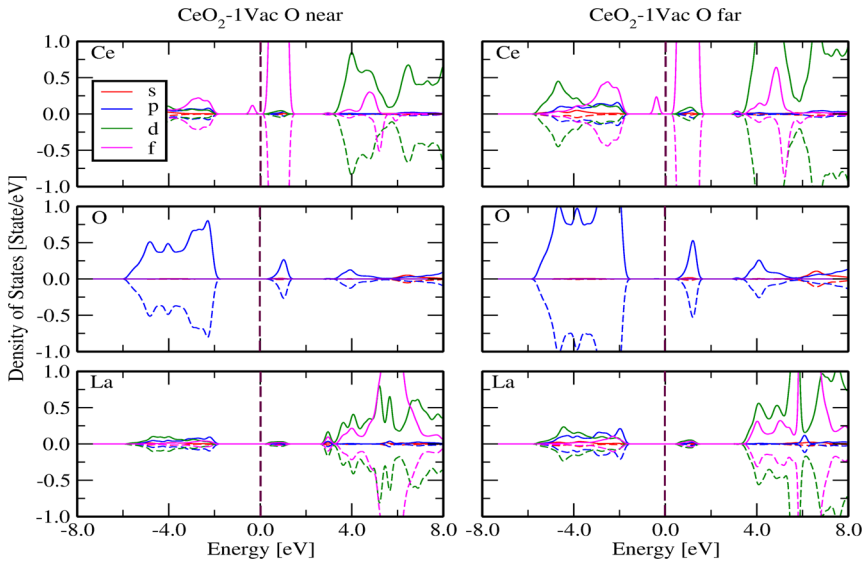

Figure 8. Density of states of cerium oxide doped by a lanthanum impurity with an oxygen deficiency near (left panel) and far (right panel) from the lanthanum. The Fermi energy is taken as 0.0 eV.

DOI: 10.1021/acs.jpcc.9b07217
J. Phys. Chem. C 2020, 124, 997−1007

calculations are strictly related to eqs 1−20, helping us to understand the weight of each path in the transport properties of pure and La-doped CeO_2 with electrons injected in the structure by defect equilibria having the possibility to spend their time on Ce, La, or oxygen vacancies. Having a look at Figure 8, one can see that the Ce-DoS around 1 eV is much larger than that of La; therefore, we can conclude that most of the time, the electrons are likely to stay in $[Ce^{3+}] \gg [La^{3+}]$.

In this way, our system is predominantly composed of oxygen vacancies near the lanthanum atoms whose f-level energies are shifted from the Fermi level, in good agreement with the previous results reported by Thorat et al.,[52] Deguchi et al.,[53] and Yoshida et al.[54] In addition, according to the electrical transport defined by the cluster-to-cluster charge transfer (CCCT),[62,63] the probability of a hopping/tunneling transition is determined by the distance between the available sites and potential barrier to be overcome. If the distance is longer than 10 Å, then an electron would hop rather than tunnel.[55,64] Therefore, considering the unit cell given in Figure 7 with an experimental lattice parameter (a) of approximately 5 Å, the electrical transport within the structure and along the first neighbors would be predominantly composed of tunneling electrons along defective Ce(III) species, whereas the transfer of electrons throughout the bulk would be virtually achieved by hopping processes.

4. CONCLUSIONS

The combination of experimental and theoretical approaches to understand the electrical behavior of our CeO_2-based samples revealed that the hopping/tunneling of electrons in the 4f states must be considered being the responsible mechanism of the CCCT electrical conduction, along with the lanthanum intermediate-energy f-states. The presence of multitraps was confirmed, which depended on the described equilibrium between the oxygen vacancies ($V_o^x \leftrightarrow V_O^{\cdot} \leftrightarrow V_O^{\cdot}$) as well as on their interaction in the distinct defective clusters with available electronic density for conduction. The modification with lanthanum increased the electrical resistance of the system, although the voltage coefficient of resistance (VCR) decreased, which was interpreted as a consequence of the decrease in the number of Ce(III) species. This was a good indicator that electrons from Ce $4f^1$ states decayed to La f-states. Indeed, doping CeO_2 with lanthanum generated more ionized oxygen vacancies close to the lanthanum atoms. The new formed La f-states induced the Ce(III) species to undergo oxidation to Ce(IV) owing to the Fermi level shifting. Thus, relatively fewer electrons in the 4f states were available for electrical conduction, increasing its total electrical resistance. The film capacitance in both the atmospheres and at the applied voltages was reduced, indicating a decrease in the density of the defective Ce(III) species possessing itinerant 4f electrons responsible for the electrical conduction mechanism. Therefore, we showed that the frequency dependence of the total resistance and capacitance could be associated with the presence of deep bulk traps (polarons), which in turn were ascribed to the interactions of the defective oxygen and rare-earth species throughout the system, corroborating the cluster-to-cluster charge transfer (CCCT) mechanism. Additionally, according to the theoretical investigations, our system was predominantly conformed of oxygen vacancies located near from the lanthanum atoms whose f-level energies shifted from the Fermi level. Furthermore, according to the electrical transport defined by the CCCT probability of the hopping transition, and consideration of the unit cell with an experimental lattice parameter (a) of approximately 5 Å, the electrical transport within the unit cell and along the first neighbors would be predominantly composed of tunneling electrons. By contrast, the transfer of electrons throughout the bulk would be virtually achieved by hopping processes with the oxygen vacancies playing the major role in the conductivity of the ceria-based materials.

AUTHOR INFORMATION

Corresponding Author

*E-mail: leandro.rocha@liec.ufscar.br.

ORCID

Leandro S. R. Rocha: 0000-0002-6059-2197

Luis Cabral: 0000-0002-4834-0552

Elson Longo: 0000-0001-8062-7791

Author Contributions

The manuscript was written through contributions of all authors. All authors have given approval to the final version of the manuscript.

Funding

CAPES, CNPq, FAPESP.

Notes

The authors declare no competing financial interest.

ACKNOWLEDGMENTS

The authors thank the following Brazilian agencies for their financial support of this research project: “Coordenação de Aperfeiçoamento de Pessoal de Nível Superior”, Brazil (CAPES), finance code 001, the National Council for Scientific and Technological Development (CNPq), and “Fundação de Amparo à Pesquisa do Estado de São Paulo” (FAPESP), grant nos. 2013/07296-2 (CEPID), 2014/19142-2, 2016/25500-4, 2017/19143-7, 2018/20729-9, and 2018/20590-0.

REFERENCES

(1) Wang, L.-S.; Li, C.-X.; Li, C.-J.; Yang, G.-J. Performance Of $La_{0.8}Sr_{0.2}Ga_{0.8}Mg_{0.2}O_3$-Based SOFCs With Atmospheric Plasma Sprayed La-Doped CeO_2 Buffer Layer. *Electrochim. Acta* **2018**, *275*, 208−217.

(2) Hussain, S.; Aslam, N.; Yang, X. Y.; Javed, M. S.; Xu, Z.; Wang, M.; Liu, G.; Qiao, G. Unique Polyhedron CeO_2 Nanostructures For Superior Formaldehyde Gas-Sensing Performances. *Ceram. Int.* **2018**, *44*, 19624−19630.

(3) Singh, K.; Kumar, K.; Srivastava, S.; Chowdhury, A. Effect Of Rare-Earth Doping In CeO_2 Matrix: Correlations With Structure, Catalytic And Visible Light Photocatalytic Properties. *Ceram. Int.* **2017**, *43*, 17041−17047.

(4) Chen, M.; Gao, H.; Zhang, L.; Xuan, Y.; Ren, J.; Ni, M.; Lin, Z. Unlocking The Nature Of The Co-Doping Effect On The Ionic Conductivity Of CeO_2-Based Electrolyte. *Ceram. Int.* **2019**, *45*, 3977−3985.

(5) Nagaraju, P.; Vijayakumar, Y.; Radhika, P.; Choudhary, R. J.; RamanaReddy, M. V. Structural, Morphological, Optical And Gas Sensing Properties Of Nanocrystalline Ceria Thin Films. *Mater. Today: Proc.* **2016**, *3*, 4009−4018.

(6) Marabelli, F.; Wachter, P. Covalent Insulator CeO_2: Optical Reflectivity Measurements. *Phys. Rev. B* **1987**, *36*, 1238−1243.

(7) Tiwari, S.; Rathore, G.; Patra, N.; Yadav, A. K.; Bhattacharya, D.; Jha, S. N.; Tseng, C. M.; Liu, S. W.; Biring, S.; Sen, S. Oxygen And Cerium Defects Mediated Changes In Structural, Optical And Photoluminescence Properties Of Ni Substituted CeO_2. *J. Alloys Compd.* **2019**, *782*, 689−698.

DOI: 10.1021/acs.jpcc.9b07217
J. Phys. Chem. C 2020, 124, 997−1007

(8) Mittal, M.; Gupta, A.; Pandey, O. P. Role Of Oxygen Vacancies In Ag/Au Doped CeO_2 Nanoparticles For Fast Photocatalysis. *Sol. Energy* **2018**, *165*, 206−216.
(9) Sun, Q.; Fu, Z.; Yang, Z. Effects Of Rare-Earth Doping On The Ionic Conduction Of CeO_2 In Solid Oxide Fuel Cells. *Ceram. Int.* **2018**, *44*, 3707−3711.
(10) Esch, F.; Fabris, S.; Zhou, L.; Montini, T.; Africh, C.; Fornasiero, P.; Comelli, G.; Rosei, R. Electron Localization Determines Defect Formation On Ceria Substrates. *Science* **2005**, *309*, 752−755.
(11) Tuller, H. L.; Nowick, A. S. Small Polaron Electron Transport In Reduced CeO_2 Single Crystals. *J. Phys. Chem. Solids* **1977**, *38*, 859−867.
(12) Rao, G. V. S.; Ramdas, S.; Mehrotra, P. N.; Rao, C. N. R. Electrical Transport In Rare-Earth Oxides. *J. Solid State Chem.* **1970**, *2*, 377−384.
(13) Huang, S.; Li, L.; Van Der Biest, O.; Vleugels, J. Influence Of The Oxygen Partial Pressure On The Reduction Of CeO_2 And CeO_2ZrO_2 Ceramics. *Solid State Sci.* **2005**, *7*, 539−544.
(14) Blumenthal, R. N.; Hofmaier, R. L. The Temperature And Compositional Dependence Of The Electrical Conductivity Of Nonstoichiometric CeO_{2-X}. *J. Electrochem. Soc.* **1974**, *121*, 126.
(15) Blumenthal, R. N.; Sharma, R. K. Electronic Conductivity In Nonstoichiometric Cerium Dioxide. *J. Solid State Chem.* **1975**, *13*, 360−364.
(16) Kullgren, J.; Castleton, C. W. M.; Müller, C.; Ramo, D. M.; Hermansson, K. B3lyp Calculations Of Cerium Oxides. *J. Chem. Phys.* **2010**, *132*, No. 054110.
(17) Kotani, A.; Parlebas, J. C. Core Photoemission Theory Of Semiconducting Rare Earth Compounds. *J. Phys.* **1985**, *46*, 77−82.
(18) Hitchcock, P. B.; Lappert, M. F.; Maron, L.; Protchenko, A. V. Lanthanum Does Form Stable Molecular Compounds In The +2 Oxidation State. *Angew. Chem., Int. Ed.* **2008**, *47*, 1488−1491.
(19) Milberg, B.; Juan, A.; Irigoyen, B. Redox Behavior Of A Low-Doped Pr-CeO_2(111) Surface. A DFT+U Study. *Appl. Surf. Sci.* **2017**, *401*, 206−217.
(20) Rocha, L. S. R.; Cilense, M.; Ponce, M. A.; Aldao, C. M.; Oliveira, L. L.; Longo, E.; Simoes, A. Z. Novel Gas Sensor With Dual Response Under $CO_{(g)}$ Exposure: Optical And Electrical Stimuli. *Phys. B* **2018**, *536*, 280−288.
(21) Hong, S. J.; Virkar, A. V. Lattice Parameters And Densities Of Rare-Earth Oxide Doped Ceria Electrolytes. *J. Am. Ceram. Soc.* **1995**, *78*, 433−439.
(22) Ortega, P. P.; Rocha, L. S. R.; Cortés, J. A.; Ramirez, M. A.; Buono, C.; Ponce, M. A.; Simões, A. Z. Towards Carbon Monoxide Sensors Based On Europium Doped Cerium Dioxide. *Appl. Surf. Sci.* **2019**, *464*, 692−699.
(23) Deus, R. C.; Amoresi, R. A. C.; Desimone, P. M.; Schipani, F.; Rocha, L. S. R.; Ponce, M. A.; Simoes, A. Z.; Longo, E. Electrical Behavior Of Cerium Dioxide Films Exposed To Different Gases Atmospheres. *Ceram. Int.* **2016**, *42*, 15023−15029.
(24) Glycerin Producers' Association, *Physical Properties Of Glycerine And Its Solutions*; Glycerine Producers' Association: New York, 1963.
(25) Hohenberg, P.; Kohn, W. Inhomogeneous Electron Gas. *Phys. Rev.* **1964**, *136*, B864−B871.
(26) Kohn, W.; Sham, L. J. Self-Consistent Equations Including Exchange And Correlation Effects. *Phys. Rev.* **1965**, *140*, A1133.
(27) Perdew, J. P.; Burke, K.; Ernzerhof, M. Generalized Gradient Approximation Made Simple. *Phys. Rev. Lett.* **1996**, *77*, 3865−3868.
(28) Blöchl, P. E. Projector Augmented-Wave Method. *Phys. Rev. B* **1994**, *50*, 17953−17979.
(29) Kresse, G.; Joubert, D. From Ultrasoft Pseudopotentials To The Projector Augmented-Wave Method. *Phys. Rev. B* **1999**, *59*, 1758−1775.
(30) Kresse, G.; Furthmüller, J. Efficient Iterative Schemes ForAb InitioTotal-Energy Calculations Using A Plane-Wave Basis Set. *Phys. Rev. B* **1996**, *54*, 11169−11186.
(31) Hafner, J. Materials simulations using VASP: a quantum perspective to materials science. *Comput. Phys. Commun.* **2007**, *177*, 6−13.
(32) Alaydrus, M.; Sakaue, M.; Kasai, H. A DFT+U Study On The Contribution Of 4f Electrons To Oxygen Vacancy Formation And Migration In Ln-Doped CeO_2. *Phys. Chem. Chem. Phys.* **2016**, *18*, 12938−12946.
(33) Chen, H. T. First-Principles Study Of Co Adsorption And Oxidation On Ru-Doped CeO_2(111) Surface. *J. Phys. Chem. C* **2012**, *116*, 6239−6246.
(34) Keating, P. R. L.; Scanlon, D. O.; Morgan, B. J.; Galea, N. M.; Watson, G. W. Analysis Of Intrinsic Defects In CeO_2 Using A Koopmans-Like GGA+U Approach. *J. Phys. Chem. C* **2012**, *116*, 2443−2452.
(35) Boella, G.; Galliana, F. Analysis of the voltage coefficient of high value standard resistors. *Measurement* **2008**, *41*, 1−9.
(36) Pike, G. E.; Seager, C. H. The Dc Voltage Dependence Of Semiconductor Grain-Boundary Resistance. *J. Appl. Phys.* **1979**, *50*, 3414−3422.
(37) Heinmaa, I.; Joon, T.; Kooskora, H.; Pahapill, J.; Subbi, J. Local Structure And Oxygen Ion Dynamics In La Doped Ceria: 17O NMR Study. *Solid State Ionics* **2010**, *181*, 1309−1315.
(38) O'Neill, W. M.; Morris, M. A. The Defect Chemistry Of Lanthana−Ceria Mixed Oxides By MASNMR. *Chem. Phys. Lett.* **1999**, *305*, 389−394.
(39) Liu, L.; Wang, X.; Guo, M.; Zhang, M. Kinetics Investigation Of Oxygen Storage Capacity In La_2O_3−CeO_2 Solid Solution. *J. Nanosci. Nanotechnol.* **2011**, *11*, 2155−2162.
(40) Ponce, M. A.; Castro, M. S.; Aldao, C. M. Capacitance And Resistance Measurements Of SnO_2 Thick-Films. *J. Mater. Sci.: Mater. Electron.* **2009**, *20*, 25−32.
(41) Deus, R. C.; Cortés, J. A.; Ramirez, M. A.; Ponce, M. A.; Andres, J.; Rocha, L. S. R.; Longo, E.; Simões, A. Z. Photoluminescence Properties Of Cerium Oxide Nanoparticles As A Function Of Lanthanum Content. *Mater. Res. Bull.* **2015**, *70*, 416−423.
(42) Ponce, M. A.; Castro, M. S.; Aldao, C. M. Influence Of Oxygen Adsorption And Diffusion On The Overlapping Of Intergranular Potential Barriers In SnO_2 Thick Films. *Mater. Sci. Eng.* **2004**, *111*, 14−19.
(43) Li, C.; Domen, K.; Maruya, K.-I.; Onishi, T. Oxygen Exchange Reactions Over Cerium Oxide: An FT-IR Study. *J. Catal.* **1990**, *123*, 436−442.
(44) Keating, P. R. L.; Scanlon, D. O.; Watson, G. W. The Nature Of Oxygen States On The Surfaces Of CeO_2 And La-Doped CeO_2. *Chem. Phys. Lett.* **2014**, *608*, 239−243.
(45) Kirk, C. T. A Theory Of Transistor Cutoff Frequency (f_T) Falloff At High Current Densities. In *IRE Transactions on Electron Devices*; IEEE: 1962, *9*, 164−174.
(46) Ponce, M. A.; Parra, R.; Savu, R.; Joanni, E.; Bueno, P. R.; Cilense, M.; Varela, J. A.; Castro, M. S. Impedance Spectroscopy Analysis Of TiO_2 Thin Film Gas Sensors Obtained From Water-Based Anatase Colloids. *Sens. Actuators, B* **2009**, *139*, 447−452.
(47) Chiou, B. S.; Chung, M. C. Admittance Spectroscopy And Trapping Phenomena Of ZnO Based Varistors. *J. Electron. Mater.* **1991**, *20*, 885−890.
(48) Hautojärvi, P.; Corbel, C. *Positron Spectroscopy Of Defects In Metals And Semiconductors*; Dupasquier, A., Mills, A. P., Jr., Eds.; IOP Press: 1995, Vol. *125*, pp 491−532.
(49) Liu, X.; Zhou, K.; Wang, L.; Wang, B.; Li, Y. Oxygen Vacancy Clusters Promoting Reducibility And Activity Of Ceria Nanorods. *J. Am. Chem. Soc.* **2009**, *131*, 3140−3141.
(50) Wang, L.; Yu, Y.; He, H.; Zhang, Y.; Qin, X.; Wang, B. Oxygen Vacancy Clusters Essential For The Catalytic Activity Of CeO_2 nanocubes For O-xylene Oxidation. *Sci. Rep.* **2017**, *7*, 12845.
(51) Sachdeva, A.; Chavan, S. V.; Goswami, A.; Tyagi, A. K.; Pujari, P. K. Positron Annihilation Spectroscopic Studies On Nd-Doped Ceria. *J. Solid State Chem.* **2005**, *178*, 2062−2066.

DOI: 10.1021/acs.jpcc.9b07217
J. Phys. Chem. C 2020, 124, 997−1007

(52) Thorat, A. V.; Ghoshal, T.; Holmes, J. D.; Nambissan, P. M. G.; Morris, M. A. A Positron Annihilation Spectroscopic Investigation Of Europium-Doped Cerium Oxide Nanoparticles. *Nanoscale* **2014**, *6*, 608−615.
(53) Yoshida, H.; Deguchi, H.; Miura, K.; Horiuchi, M.; Inagaki, T. Investigation of the relationship between the ionic conductivity and the local structures of singly and doubly doped ceria compounds using EXAFS measurement. *Solid State Ionics* **2001**, 191−199.
(54) Deguchi, H.; Yoshida, H.; Inagaki, T.; Horiuchi, M. EXAFS study of doped ceria using multiple data set fit. *Solid State Ionics* **2005**, 1817−1825.
(55) Barsan, N.; Weimar, U. Fundamentals Of Metal Oxide Gas Sensors. In *14th International Meeting on Chemical Sensors*; AMA-Science: 2012, 618−621.
(56) Zacherle, T.; Schriever, A.; De Souza, R. A.; Martin, M. Ab Initio Analysis Of The Defect Structure Of Ceria. *Phys. Rev. B* **2013**, *87*, 134104.
(57) Žguns, P. A.; Ruban, A. V.; Skorodumova, N. V. Phase diagram and oxygen-vacancy ordering in the CeO_2-Gd_2O_3 system: a theoretical study. *Phys. Chem. Chem. Phys.* **2018**, *20*, 11805−11818.
(58) Žguns, P. A.; Ruban, A. V.; Skorodumova, N. V. Ordering and phase separation in Gd-doped ceria: a combined DFT, cluster expansion and Monte Carlo study. *Phys. Chem. Chem. Phys.* **2017**, *19*, 26606−26620.
(59) Grope, B.O.H.; Zacherle, T.; Nakayama, M.; Martin, M. Oxygen ion conductivity of doped ceria: A Kinetic Monte Carlo study. *Solid State Ionics* **2012**, *225*, 476−483.
(60) Koettgen, J.; Grieshammer, S.; Hein, P.; Grope, B. O. H.; Nakayama, M.; Martin, M. Understanding the ionic conductivity maximum in doped ceria: trapping and blocking. *Phys. Chem. Chem. Phys.* **2018**, *20*, 14291−14321.
(61) Grieshammer, S.; Grope, B. O. H.; Koettgen, J.; Martin, M. A combined DFT + U and Monte Carlo study on rare earth doped ceria. *Phys. Chem. Chem. Phys.* **2014**, *16*, 9974−9986.
(62) Longo, V. M.; Cavalcante, L. S.; Paris, E. C.; Sczancoski, J. C.; Pizani, P. S.; Li, M. S.; Andres, J.; Longo, E.; Varela, J. A. Hierarchical Assembly of CaMoO4 Nano-Octahedrons and Their Photoluminescence Properties. *J. Phys. Chem. C* **2011**, *115*, 5207−5219.
(63) Cavalcante, L. S.; Longo, V. M.; Sczancoski, J. C.; Almeida, M. A. P.; Batista, A. A.; Varela, J. A.; Orlandi, M. O.; Longo, E.; Li, M. S. Electronic structure, growth mechanism and photoluminescence of CaWO4 crystals. *CrystEngComm* **2012**, *14*, 853−868.
(64) Electrical Conduction and Photoconduction. In *Dielectric Phenomena in Solids: With Emphasis on Physical Concepts of Electronic Processes*; Elsevier Academic Press: San Diego, 2004; pp 381−514.

DOI: 10.1021/acs.jpcc.9b07217
J. Phys. Chem. C 2020, 124, 997−1007